### Sublimation behavior of AIN in nitrogen and argon at conditions used for high-temperature annealing

Lukas Peters ■ (i); Dmitry Sergeev (ii); Christoph Margenfeld (iii); Michael Müller (iii); Andreas Waag (iii)



J. Appl. Phys. 133, 235704 (2023) https://doi.org/10.1063/5.0152054







## or se

# Sublimation behavior of AIN in nitrogen and argon at conditions used for high-temperature annealing

Cite as: J. Appl. Phys. 133, 235704 (2023); doi: 10.1063/5.0152054

Submitted: 27 March 2023 · Accepted: 1 June 2023 ·

Published Online: 16 June 2023 · Publisher error corrected: 21 June 2023







AFFILIATIONS

<sup>1</sup>Institute of Semiconductor Technology, Technische Universität Braunschweig, Hans-Sommer-Straße 66, Braunschweig D-38106, Germany

Lukas Peters, <sup>1,2,a)</sup> Dmitry Sergeev, <sup>3</sup> Christoph Margenfeld, <sup>1,2</sup> Michael Müller, <sup>3</sup> and Andreas Waag<sup>1,2</sup> Christoph Margenfeld, <sup>1,2</sup> C

- <sup>2</sup>Laboratory for Emerging Nanometrology (LENA), Technische Universität Braunschweig, Langer Kamp 6, Braunschweig D-38106, Germany
- Institute of Energy and Climate Research, IEK-2, Forschungszentrum Jülich GmbH, Wilhelm-Johnen-Straße, Jülich D-52428, Germany

#### **ABSTRACT**

High-temperature annealing (HTA) is one of the most promising techniques to produce high-quality, cost-efficient AlN templates for further epitaxial growth of AlGaN devices. Unfortunately, the yield of this process seems to be limited due to the restricting face-to-face configuration that is typically used, in which contaminations of the template surface can occur easily. A high yield is crucial for process transfer into industry. Indeed, templates that are annealed in open-face configuration suffer from surface degradation due to excessive AlN evaporation during the course of the annealing process. To highlight the physics that are restricting the open-face approach of the process, sublimation behavior of AlN at temperatures and atmospheres typically used in HTA processes has to be examined. In this study, we use the Knudsen effusion mass spectrometry technique to confirm the previously published results on equilibrium partial pressures of species above AlN. Based on the experimentally determined data and further AlN sublimation experiments, the apparent sublimation coefficient of AlN in N<sub>2</sub> and Ar atmospheres at HTA process conditions can be derived. Despite N<sub>2</sub> having a stabilizing effect on AlN during HTA, the still high decomposition rates of several hundred nanometers per hour can explain the excessive damage that is typically observed if AlN/sapphire templates are annealed in an open-face configuration. Finally, based on theoretical considerations, a strategy to reduce the sublimation of AlN during HTA in open-face configuration is suggested.

© 2023 Author(s). All article content, except where otherwise noted, is licensed under a Creative Commons Attribution (CC BY) license (http://creativecommons.org/licenses/by/4.0/). https://doi.org/10.1063/5.0152054

#### I. INTRODUCTION

In the past few decades, light-emitting diodes (LEDs) based on group III-nitride semiconductors have played a key role in the evolution of lighting technology. Blue light from GaN LEDs is partially converted into yellow light using phosphors, leading to white-emitting LEDs. In addition to the highly optimized and commercialized blue-emitting LEDs, solid-state emitters for the UV range received great interest lately due to the restrictions imposed on gas discharge lamps based on mercury. Specifically, a great application potential for LEDs emitting in the UV-C regime exists. UV-C radiation is suited for disinfection/sterilization purposes since germicidal efficacy of photons is the largest around an emission wavelength of 265 nm. In terms of luminescence efficiency, however,

LEDs emitting in the UV-C regime lag far behind their blue and UV-A pendants due to physical restrictions as well as technological challenges, compared to their GaN/InGaN-based counterparts that have to be surpassed. <sup>2,5,6</sup> To name a few, higher sensitivity to threading dislocations (TDs) and point defects hampers the efficacy, low transparency of the AlN growth substrates due to intrinsic point defects, light outcoupling due to changes in polarization of the photons, doping, as well as processing challenges after epitaxial growth of the LED stack due to a stronger wafer bow caused by a higher mismatch of the thermal expansion coefficient between AlN and the commonly used sapphire substrates. <sup>2,4–8</sup>

Most of the time, not all listed challenges can be tackled simultaneously. Growth on bulk AlN wafers solves problems regarding TD density and processing since the wafer bow is lower

a)Author to whom correspondence should be addressed: lukas.peters@tu-braunschweig.de

compared to the growth on sapphire and only occurs once AlN is alloyed with GaN to form AlGaN layers. Unfortunately, bulk AlN has strong absorption lines in the UV-C is expensive, and wafers are only available in small diameters, which is crucial for an industry driven by cost-per-area arguments. On the other hand, the bow problem with templates on sapphire is most severe at larger diameters.<sup>2,9</sup> Thus, bulk AlN cannot compete with AlN-on-sapphire templates up until today for UV LED applications. AlN templates that are grown using metalorganic vapor phase epitaxy (MOVPE), which is the most widely used tool for epitaxial growth of commercial semiconductor devices, are inexpensive and more transparent, but the TD density is high and can only be lowered by using elaborate processes like structuring of the wafer (e.g., nano-patterned sapphire substrates, NPSS) or the AlN layer (e.g., epitaxially lateral overgrowth, ELOG) with subsequent regrowth on top of the etched structures.<sup>2,10,11</sup> A new promising technology for achieving highquality AlN templates for subsequent LED fabrication is the so-called high-temperature annealing (HTA) of thin AlN layers on sapphire, which was introduced first by Fukuyama et al. and, subsequently, further developed by Miyake et al. by proposing the face-to-face annealing approach to reduce thermal decomposition of AlN. 12,13 HTA AlN templates solve or reduce many of the problems discussed above and are a well-suited candidate for the growth of UV-C LEDs. 14,15 Nonetheless, the face-to-face approach also exhibits certain restrictions. It is prone to contaminations introduced by mechanical stacking of the wafers for face-to-face annealing, thus hard to automate and integrate into the existing semiconductor plants.

To further develop the face-to-face approach into an open-face configuration and, thus, possibly overcome the existing restrictions, a deep understanding of the underlying mechanisms and limitations of AlN high-temperature decomposition is required. As sublimation is concerned, the literature suggests a rather simple chemical reaction for dissociation and condensation: 2 AlN  $\leftrightarrow$  2 Al + N<sub>2</sub>. <sup>16,17</sup> In addition to Al and N2, no other species are expected to be present above a heated solid AlN sample at the investigated temperatures in thermodynamic equilibrium.<sup>17</sup> Of course, models which are entirely based on equilibrium conditions cannot give information about the kinetics during HTA. Nonetheless, the fact that thin AlN layers on sapphire are stable in a face-to-face configuration at temperatures up to about 2000 K<sup>13,18</sup> (1700 °C is a typical HTA temperature used for AlN) implies that the micro-atmosphere between the two layers is buffered to some extent with decomposition products, which prevents further sublimation. In this paper, we want to examine the stabilizing mechanism and—based on our findings discuss possibilities to achieve a process that is stable without the restricting face-to-face configuration.

Equilibrium vapor pressures of pure compounds were intensively measured in the second half of the 20th century, mainly by using Knudsen effusion mass spectrometry (KEMS). Nowadays, these results are easily available in thermodynamic databases as a function of Gibbs free energy for solid, liquid, and gas phases, which allows to predict or reproduce experimental results. To access this information, different software packages based on the CALPHAD method can be used, e.g., FactSage. 19 The quality of such databases is continuously reviewed by ongoing research and relies on confirmation of the existing experimental data for the considered components. In the case of AlN, the FactPS database is used for the calculation of equilibrium partial pressures of Al and N2 species, which is surprisingly high for a material that is typically used for high-temperature applications. The same calculations were performed also for Al2O3, which is another well-established hightemperature ceramic. Al<sub>2</sub>O<sub>3</sub> has roughly seven orders of magnitude lower equilibrium partial pressure of aluminum above the solid phase at temperatures regularly used for the described HTA process. In comparison, the partial pressure of aluminum above a solid AlN sample is expected to reach 10 Pa already at roughly T = 1800 K, where the aluminum pressure above  $Al_2O_3$  should be only  $10^{-5}$  Pa.<sup>1</sup> These high values for the partial pressure of aluminum in thermal equilibrium above AlN may explain the problematic decomposition of the very thin AlN layers, which typically consist of some 100 nm thick sputtered AlN, if not annealed in a face-to-face configuration. 12,20,21

In the course of this study, we will discuss the KEMS results for high-quality single-crystalline AlN and compare them with the calculated results using FactSage. Subsequently, the measured and calculated partial pressures of AlN and Al<sub>2</sub>O<sub>3</sub> will be used to fit the measured sublimation rates of AlN during typical HTA conditions. Based on our findings, we will discuss the aforementioned limitations of the HTA process and suggest a more stable and contaminationresilient process compared to the state-of-the-art face-to-face approach.

#### **II. BASICS**

Although KEMS is a long-established measurement tool, it is not widely used in the applied semiconductor research community today. The following section, therefore, presents an introduction  $\frac{9}{8}$ to this powerful thermodynamic measurement technique.

In KEMS measurements, a small amount of the sample material is heated in a Knudsen cell. In semiconductor technology, Knudsen cells are known for molecular beam epitaxy systems. The physics of Knudsen cells is based on the studies of molecular gas flow in the early 20th century by Knudsen and amply described by Hilpert in his review from 1991.<sup>23</sup> During KEMS measurements, the molecular beam of the sample material is directed into a mass spectrometer. A typical Knudsen cell contains at least one crucible made of a suited material that is chemically inert against the sample, heating filaments, thermal shielding, and an outer cooling system. The small size of the orifice inside the lid of the cell allows the effusion of a molecular beam, which consists of species from the sample material. If Knudsen conditions are fulfilled, one can assume thermodynamic equilibrium inside of the cell, and thus, the concentration of each species in the molecular beam represents the activity of the corresponding species in equilibrium above the solid phase of the sample. Therefore, KEMS can be used to measure the equilibrium vapor pressures of the involved species above the solid sample after calibration. Figure 1 shows a generalized layout drawing of a KEMS system including all essential components.

The method of evaluating the equilibrium partial pressure or the activity has been well described in the literature.<sup>24</sup> If one uses the method discussed by Hilpert, Kobertz et al., and Sergeev et al., the equilibrium partial pressure  $p_{i,eq}$  of a species i can be calculated

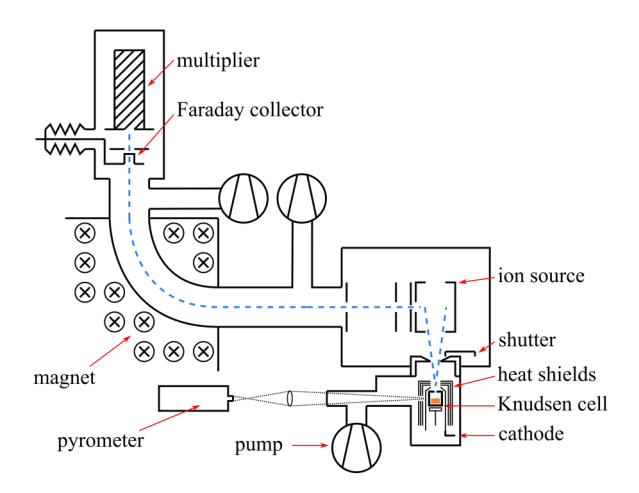


FIG. 1. Schematic representation of a typical KEMS system using a single-focusing magnetic sector field. The sample material is evaporated within a shielded Knudsen cell, which is heated by electron bombardment. A slit in the shielding allows us to measure the temperature using a pyrometer. During evaporation, a molecular beam can leave the cell, is ionized in a second vacuum chamber and, subsequently, accelerated into a magnetic sector field that filters the masses. Finally, an ion-counting system measures the intensity of the selected species.

from the measured ion intensity  $I_i$  at a given temperature T using Eq. (1),  $^{23,25,26}$ 

$$p_{i,eq} = k \; \frac{I_i \; T}{\sigma_i \; \eta_i \; \gamma_i} \; . \tag{1}$$

Additional parameters are the system calibration factor k, which is equal for all species and needs to be determined for the used Knudsen cell, the ionization cross section  $\sigma_i$ , the isotopic abundance  $\eta_i$ , and the multiplication factor  $\gamma_i$ , which is unity for an ion-counting system. The ion intensity  $I_i$  and the ionization cross section  $\sigma_i$  are functions of the ionization energy. Finally, T is the temperature of the sample. In KEMS measurements, the ionization energy is typically fixed to 70 eV, since the ionization efficiency and, thus, the cross section  $\sigma_i$  of most elements do not vary strongly in an interval around this energy. Still, identifying correct values for the ionization cross section is difficult. The calculated results from Drowart  $et\ al.$  are used regularly.

Knowing the equilibrium partial pressure  $p_{i,eq}$  of a species i allows us to use the Hertz-Langmuir-Knudsen (HLK) equation to predict the sublimation rate of a solid into the gas phase. The HLK equation as it is shown in Eq. (2) has the dimension of a mass flux per area,

$$q_i = \sqrt{\frac{m_i}{2\pi k_B T}} \left( \alpha_{i,s} \ p_{i,eq} - \alpha_{i,c} \ p_{i,sys} \right). \tag{2}$$

In Eq. (2),  $q_i$  is the material loss due to the sublimation of species i,  $m_i$  is the mass of the species i,  $k_B$  is the Boltzmann factor,  $\alpha_{i,s}$  and  $\alpha_{i,c}$  are the sublimation or condensation coefficients of

species i, and  $p_{i,eq}$  and  $p_{i,sys}$  are the equilibrium vapor pressure directly above the sample and the partial vapor pressure of species i in the system, respectively. In epitaxial growth, the condensation coefficient is also known as the so-called sticking coefficient. Equation (2) is a simplified form of the HLK equation that assumes that the condensed and vaporized phases have the same temperature. The physical interpretation of the sublimation coefficient is as follows: It represents the fraction of atoms or molecules at the interface between both phases changing from the solid to the vapor phase. If every atom or molecule in the solid phase reaches the vapor phase,  $\alpha_{i,s}$  is unity. The coefficient represents the ratio of the actual unidirectional material flux compared to the flux determined by the classical kinetic theory.<sup>29</sup> Therefore,  $\alpha_{i,s}$  is usually smaller than unity with values between 0 and 1. The same considerations are valid for the condensation coefficient but for a unidirectional mass flux toward the solid phase instead. For the purpose of simplicity, in this study, both coefficients are assumed to be equal  $(\alpha_{i,s} = \alpha_{i,c})$ . Thus, the sublimation flux is only determined by the difference in partial vapor pressure between the thin boundary layer directly above the sample and the partial pressure in the system. Anyway, only huge differences between both coefficients may influence the results of the HLK equation in this study, since the background vapor pressure in our system and the measured equilibrium vapor pressure of the sample differ by up to seven orders of magnitude at an annealing temperature.

#### **III. EXPERIMENTAL SECTION**

All experiments were conducted using commercially available AlN single crystal wafers (HexaTech, Inc.) or their fragments for the KEMS measurements. The wafers used for sublimation experiments in different atmospheres had a diameter of one inch.

KEMS measurements were performed in the facilities at FZ & Jülich. During measurements, the temperature was controlled with a W-W/26%Re thermocouple and an Impac IGA 12 pyrometer. Detection of ions was performed using a continuous dynode multiplier connected to an ion-counting system. For ionization of the molecular beam, an energy of 70 eV and an emission current of 0.15 mA were used. The ionization cross sections for all elements are taken from Drowart et al.<sup>28</sup>:  $E_{i,N} = 1.52 \text{ Å}^2$ ,  $E_{i,Al} = 6.18 \text{ Å}^2$ , and  $E_{i,N_2} = 1.93 \text{ Å}^2$ . All measurements were performed automatically by using a temperature control program with set measurement intervals and heating rates. The KEMS system was calibrated by measuring the onset of the melting temperature of pure nickel and its well-known equilibrium partial pressures for a temperature interval around the melting point. For the measurements, an AlN sample was placed inside a tungsten crucible with a graphite lid. An orifice in the graphite lid allowed a molecular beam to leave the crucible. Before measuring polythermal data, the long-time stability of the system was ensured by measuring the ion intensities of Al and N<sub>2</sub> isothermally over 60 h. The ion intensities showed a drift similar to the measured temperature drift, thus a long-time stable sample can be assumed, especially over the course of a comparably short polythermal measurement.

To supplement the KEMS experiments, AlN bulk crystals were also annealed in an open-face configuration in a furnace that is routinely used to perform face-to-face annealing processes with

AlN-on-sapphire templates. The sublimation rates of the bulk AlN wafer were derived from the weight of the wafer before and after the annealing experiments measured using a Mettler-Toledo XPR205DR precision balance. The AlN crystals were held at dwell temperature for up to 60 h, depending on the used temperature. Additional reference processes without dwell time to subtract the mass loss from the respective temperature ramp were performed as well. The AlN bulk crystals were annealed inside a cold-wall vacuum furnace, using N2 or Ar atmosphere at ambient pressure. All components inside the furnace consist of porous Al<sub>2</sub>O<sub>3</sub> (thermal isolation), sintered Al<sub>2</sub>O<sub>3</sub> (tube, sample-holder), and molybdenum (heater). Thus, the annealing atmosphere has a low Al partial pressure due to the low equilibrium partial pressure of Al above Al<sub>2</sub>O<sub>3</sub>, as discussed in the introduction. After loading, the furnace was evacuated to 50 mbar and purged three times with pure N<sub>2</sub> or Ar. Subsequently, the temperature controller was set to the desired temperature with a maximum heating rate of 8 K/min and the aforementioned dwell times. During annealing, the inner furnace tube was purged with the process gas. Gas flows of 1 and 5 slm were used. At the end of the program, the heater was turned off and the samples cooled passively, while purged with N2 or Ar during cooling.

#### IV. RESULTS AND DISCUSSIONS

During the isothermal measurement of the AlN single crystal, we were able to exclude the appearance of AlN or bigger molecular species in the gas phase at equilibrium conditions. The mass spectrum shown in Fig. 2 was measured at 1700 K. It reveals mainly Al<sup>+</sup> and N<sub>2</sub><sup>+</sup> ions in the gas phase at thermodynamic equilibrium. It also shows a small intensity of atomic nitrogen, which was not predicted as one of the main species by FactSage calculations.

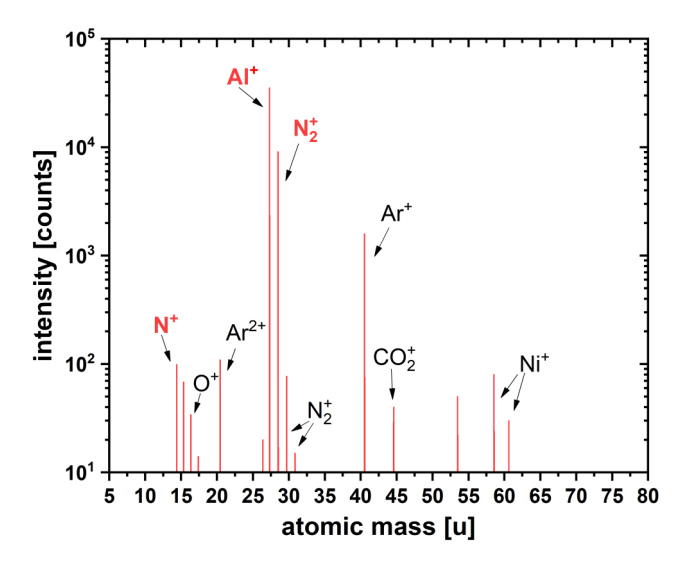


FIG. 2. A mass spectrum measured at a temperature of 1700 K revealing mainly Al and N2 and trace N above AlN. The other main peaks at atomic masses above 58 u can be related to residuals of the Ni calibration sample.

In an earlier published work on AlN also, no more complex AlN molecules were measured using the KEMS technique, but aluminum-oxygen molecules were reported, which we did not observe. 17 The absence of oxygen-containing molecules can be explained by the quality of the studied sample. State-of-the-art single-crystalline bulk AlN contains less oxygen compared to non-optimized bulk AlN or even AlN powder samples. Typical oxygen concentrations in state-of-the-art single-crystalline bulk AlN wafers are in the order of mid- $10^{18}\,\mathrm{cm}^{-3}.^{30,31}$  Nonetheless, KEMS data published in the literature of AlN-containing systems showed complexes with higher mass compared to AlN. Meloni and Gingerich measured Al<sub>2</sub>N, AlN, and Al<sub>2</sub>N<sub>2</sub> above the AlN-Au-C system, but also suggested Au to be involved in the reaction to the more complex molecules.<sup>32</sup> Andrews et al. used infrared matrix isolation spectroscopy to study the chemical reaction between atomic Al and N2 and identified AlN<sub>2</sub>, Al<sub>2</sub>N, Al<sub>2</sub>N<sub>2</sub>, AlN<sub>3</sub>, and Al<sub>3</sub>N.<sup>33</sup> However, KEMS is an equilibrium technique and does not allow statements about the involved reactions. In addition to the AlN-related signals, the mass spectrum in Fig. 2 also shows the distinct peaks of <sup>58</sup>Ni<sup>+</sup> and <sup>60</sup>Ni<sup>+</sup> with ratios respecting the isotopic distribution of Ni, stemming from the calibration process of the setup.<sup>34</sup> Masses that are presumably related to Ar2+ and atomic O were also detected. The nonlabeled masses were not assignable and may stem from unknown impurities inside either the crucible or the sample.

Figure 3(a) shows the calculated equilibrium partial pressures of all expected species above a solid AlN source in red color.<sup>1</sup> Compared to Al and N2, all other species have comparably small equilibrium partial pressures. Thus, Al and N2 can be expected as the predominant species in the gas phase above AlN. For comparison, the partial pressures of Al and O above Al<sub>2</sub>O<sub>3</sub> are also plotted in blue color. Figure 3(b) shows the results of the polythermal 8 KEMS measurement. The dashed lines in red and blue colors represent the calculated values of the equilibrium partial pressure of  $\frac{4}{50}$ Al and  $N_2$  above AlN as shown in Fig. 3(a), respectively. They agree well with the measurements (red and blue dots) roughly between 1450 and 1750 K. At the highest temperatures measured, the ion intensity of Al was exceeding the limits of the used ioncounting system, and thus, the Al intensity saturates above 1700 K. Please note that Knudsen conditions are only satisfied in a range up to 10 Pa, and thus, the KEMS technique is not viable for the AlN system at temperatures above 1700 to 1750 K, since both Al and N<sub>2</sub> exceed 10 Pa above this range.<sup>23</sup> At low temperatures, the N<sub>2</sub> signal deviates from the FactSage calculations, since N<sub>2</sub> usually shows a rather strong background signal in the used system. Interestingly, the measured equilibrium partial pressure for atomic nitrogen is rather high. This was not expected based on the available FactSage data shown in Fig. 3(a). Using Clausius Clapeyron's equation, the enthalpy of vaporization  $\Delta H_{vap}$  of AlN can be calculated from our experimental data as shown in Fig. 3(b). It is widely accepted that AlN evaporates congruently if a thermodynamic equilibrium is present.<sup>9,35,36</sup> Thus, if AlN sublimates congruently, the slopes should be identical. The results of the fitting procedure are shown in Table I. Our obtained values are deviating by up to 15.2% from the FactSage value of 179.74 kJmol<sup>-1</sup>, in the case of Al partial pressure. However, since our set of data is limited in size, we do not want to challenge the values deposited in the FactPS database. Thus, we want to attribute our measured deviation either to

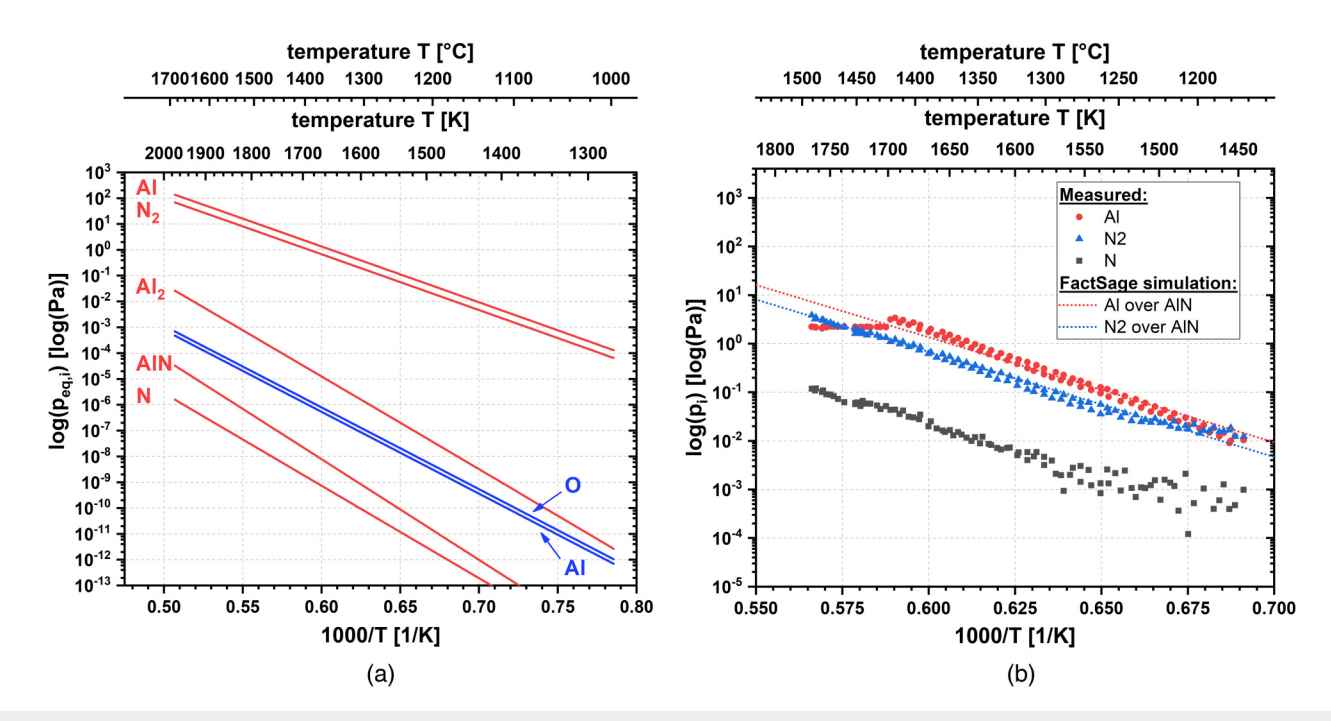


FIG. 3. (a) Calculated equilibrium partial pressures of selected species above AIN (red) and Al<sub>2</sub>O<sub>3</sub> (blue) using FactSage. (b) Measured partial pressures above AIN using KEMS (dots) with the respective FactSage calculations for Al and N2 (dashed lines) as a comparison. The dashed lines in (b) correspond to the partial pressures of Al and N2 in (a).

statistical errors due to a small sample size or the volume inside the Knudsen cell that may not have reached equilibrium, and therefore, the solid AlN evaporated incongruently during our measurement.

Based on the available Al and N2 FactSage data, one has to expect partial pressures of  $p_{eq, Al} \approx 137.7 \, \text{Pa}$  and  $p_{eq, N_2} \approx 68.9 \, \text{Pa}$  at typically used temperatures of 1973.15 K in between two wafers in face-to-face configuration during an HTA process, if equilibrium conditions apply. Following the HLK equation, annealing without the face-to-face configuration would lead to a significant mass loss of the solid phase, since the partial pressure of Al in a typically used furnace made of Al<sub>2</sub>O<sub>3</sub> or graphite is negligibly small. As discussed in Eq. (2), the main driving force of sublimation is the difference in the equilibrium pressure and the actual partial pressure in the system. In the framework of this study, a cold-wall furnace with mainly Al<sub>2</sub>O<sub>3</sub>-based inner components was used. Therefore, we suppose the background Al pressure to be equal to the equilibrium partial pressure of Al above Al<sub>2</sub>O<sub>3</sub>, as it is shown in Fig. 3(a). 19 Since a congruent sublimation process for AlN is likely, 9,35,36 the measured mass losses were corrected using the mass-ratio of atomic nitrogen  $m_{\rm N} = 2.33 \times 10^{-26} \, \rm kg$  and aluminum  $m_{\rm Al} = 4.48 \times 10^{-26} \, \rm kg$ . By comparing both masses, 65.79% of the total measured mass difference after the sublimation experiment  $\vec{\varphi}$ can be attributed to a loss of aluminum atoms from the solid & phase. For the fitting procedure with Eq. (2), the partial pressures of aluminum above AlN and Al<sub>2</sub>O<sub>3</sub> were parameterized using their temperature dependence via the standard enthalpy of formation as obtained from the FactSage database. 19 The sublimation coefficient  $\alpha_{Als}$  is used as the fitting parameter. The measured and fitted results for AlN sublimation in N2 and Ar atmosphere at different gas flows are shown in Fig. 4. The fitting parameter results are shown in Table II. Previous reports about  $\alpha_{Al,s}$  are higher in value, which would contribute to an increased mass loss during sublimation experiments. Hoch and Ramakrishnan measured a sublimation coefficient of  $5 \times 10^{-3}$  for  $N_2$ . In a second study, a value of  $2.2 \times 10^{-3}$  was published.<sup>35</sup> Since congruent vaporization of AlN is established, assuming a similar sublimation coefficient for Al is standing to reason. In a later publication, Dryburgh discussed the widely accepted value of Hoch and Ramakrishnan in the context of

TABLE I. Enthalpy of vaporization values obtained from fitting the Clausius Clapeyron's equation to the experimental data shown in Fig. 3(b), as discussed in the text.

| Vapor species   | Al                                | $N_2$                             | N                              |
|---|-----------------------------------|-----------------------------------|--------------------------------|
| Enthalpy of vaporization                                  | $207 \pm 0.7 \text{ kJ mol}^{-1}$ | $184 \pm 1.4 \text{ kJ mol}^{-1}$ | 181 ± 5.5 kJ mol <sup>-1</sup> |
| Deviation from FactPS data (179.74 kJ mol <sup>-1</sup> ) | 15.2%                             | 2.9%                              | 0.8%                           |
| Fitting range   | T < 1700 K                        | T > 1550 K                        | T > 1600 K                     |

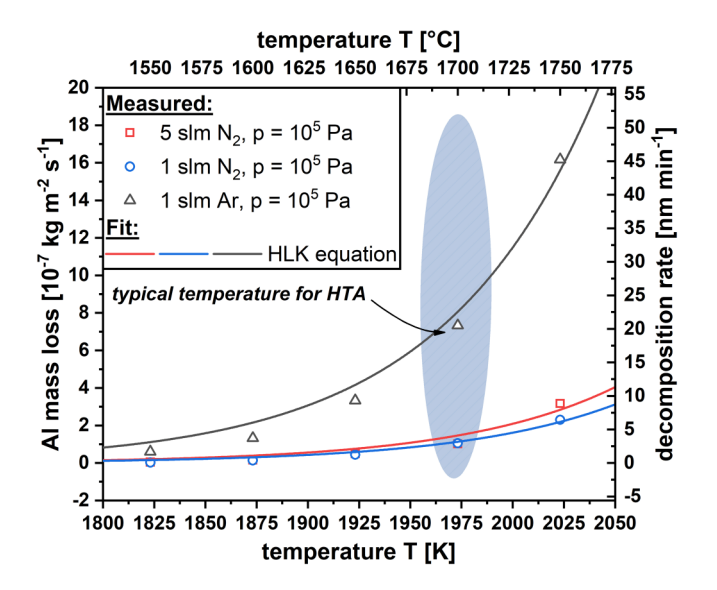


FIG. 4. Measured AI mass loss and the respective etching rate for the sublimation experiments in N<sub>2</sub> atmosphere using gas flows of 1 slm (blue) and 5 slm (red) and Ar atmosphere with a gas flow of 1 slm (gray). The solid curves are the result of the fitting procedure with the HLK equation as shown in Eq. (2) with  $\alpha_{\text{Al},\text{s}}$  as the fitting parameter.

the maximum achievable growth rates for AlN crystals by direct sublimation.<sup>39</sup> Since the HKL equation assumes a constant partial pressure in the whole system, it may oversimplify the experiment. Thus, the differences in the measured and reported coefficients may stem from a stabilizing Al-rich boundary layer above the AlN sample. This will be further examined below.

In addition to the mass loss, one can calculate the thermal etching rates of AlN using its density of  $\rho_{AlN} = 3.255 \text{ g/cm}^3$ . Many publications are using annealing temperatures during HTA in an interval around 1970 K (1680-1725 °C, as highlighted in Fig. 4). 13,18,40 Based on our findings, one has to expect a decomposition rate of up to roughly ~5 nm/min depending on the N2 flow in the given temperature regime. Using Ar as a process gas is not a reasonable choice in the studied parameter range, showing decomposition rates of ~20 nm/min. Thus, an open-face annealed AlN layer may lose several hundreds of nm layer thickness during the course of a typical HTA process in N2 atmosphere that usually takes several hours. 13,41 The separation of the two curves for annealing in 5 and 1 slm N2 (red and blue, respectively), as shown in Fig. 4, indicates that the gas flow may be a lever to reduce etching in an open-face configuration. We assume that this effect stems from advective transport of gaseous aluminum away from

TABLE II. Resulting sublimation coefficients of the fits shown in Fig. 4 using the HLK equation as it is explained and discussed in Eq. (2).

| Annealing conditions    | 1 slm N <sub>2</sub> | 5 slm N <sub>2</sub> | 1 slm Ar             |
|-------------------------|----------------------|----------------------|----------------------|
| Sublimation coefficient | $1.6 \times 10^{-6}$ | $2.1 \times 10^{-6}$ | $1.1 \times 10^{-5}$ |

the AlN sample during annealing. In other words, a loss of vaporous Al species may occur above the solid AlN due to the gas stream. Since annealing takes place at standard pressure and convective transport is the main mass transport mechanism, a relatively stable Al-rich boundary layer is formed above the wafer. Higher gas fluxes may lead to the advective transport or thinning of this boundary layer, and thus, reduce the effective Al background pressure directly above the solid AlN surface, which leads to higher sublimation rates of the sample. If the assumption of a stabilizing boundary layer at standard pressure is correct, this would also explain the effectiveness of face-to-face annealing, which is not only known from HTA, but also, for example, from conventional III-V semiconductors such as GaAs or Bi<sub>2</sub>Sr<sub>2</sub>CaCu<sub>2</sub>O<sub>x</sub> research as so-called "proximity-cap annealing". 42-46 The face-to-face or proximity-cap approach leads to N2 and Al buffered atmosphere between the two wafers, and thus, hinders the evaporation or sublimation of the respective material by simple means. Due to the nature of this geometrical configuration, process gas fluxes cannot easily disturb the atmosphere between the two wafers. At high process pressures, for example, standard pressure, the microatmosphere between both wafers seems to be stable.

Based on these considerations, we have to repeat our remark on the calculated sublimation coefficient from the fitting procedure. We assumed a constant background partial pressure of Al due to the low equilibrium partial pressure of Al above  $Al_2O_3$ . If in reality, the Al background pressure in the boundary layer is higher, we may underestimate the sublimation coefficient of AlN, as indicated above. Since the real partial pressure in the posited boundary layer would not be accessible experimentally by direct means, this apparent sublimation coefficient can still be used as a measure to compare the influence of the used gases and the gas fluxes on the HTA 8 process relative to each other. Following this argumentation, the  $\frac{4}{\omega}$  results for sublimation in the Ar atmosphere (gray curve in Fig. 4)  $\frac{4}{\omega}$ confirm that N2 has a stabilizing effect on AlN. The total sublimation rate is reduced by buffering the atmosphere with N2 compared to Ar. However, the stabilizing effect of the N2-buffered atmosphere does not compensate for the driving force of a low Al background pressure in the system. To ensure the stability of AlN, an additional gaseous Al buffer is needed if annealing takes place at normal pressure. As an alternative approach that follows Le Chatelier's principle, as it is known, e.g., from GaN technology (ultrahigh pressure annealing with pressures of up to 10<sup>9</sup> Pa),<sup>47</sup> annealing in N<sub>2</sub> overpressure could lead to a sufficient suppression of AlN decomposition. To estimate a suitable process pressure, one can calculate the reaction enthalpy of the dissociation reaction of AlN,

$$2 AlN \rightarrow 2 Al + N_2, \tag{3}$$

$$K_p = \frac{p_{\rm Al}^2 \times p_{\rm N_2}}{a_{\rm AlN}^2},$$
 (4)

$$\Delta_r G^0 = -RT \times \ln \frac{p_{\rm Al}^2 \times p_{\rm N_2}}{a_{\rm AlN}^2}.$$
 (5)

Equation (5) gives the value of the reaction enthalpy of the chemical reaction shown in Eq. (3).  $K_p$  is the equilibrium constant

of Eq. (3),  $p_{A1}$  and  $p_{N_2}$  are the partial pressures of Al and N<sub>2</sub>, respectively,  $a_{AlN}$  is the activity of the solid AlN phase, and R is the gas constant. Typically, the chemical activity of a solid is unity. At high pressures, one has to correct the value of chemical activity using Eq. (6),

$$a_{\text{AlN}} = \exp \frac{V_{\text{AlN}}(p - p_0)}{RT}.$$
 (6)

Here, p is the total pressure in the system,  $p_0$  is the standard pressure, and  $V_{AlN}$  is the molar volume of AlN. Assuming that  $V_{AlN}$  is constant and by using the density and molar mass of AlN (3.255 g/cm<sup>3</sup> and 40.989 g/mol, respectively), Eq. (6) can be used to calculate  $a_{AIN}$  for varying pressures. Indeed, this is a simplification, since high pressures will surely affect the density of AlN. Combining Eqs. (5) and (6) together with an expression for the total pressure of the system  $p = p_{Al} + p_{N_2}$ , one obtains a model that allows predictions for the stability of AlN during an annealing process using different pressures,

$$\Delta_r G^0 = -RT \times \ln \frac{p_{\text{Al}}^2 \times (p - p_{\text{Al}})}{\exp \frac{V_{\text{AlN}}(p - p_0)}{RT}}.$$
 (7)

Figure 5 shows the resulting reaction enthalpy to temperature relations for different process pressures, using the model discussed in Eq. (7). The Al partial pressure  $p_{Al}$  was parameterized using its temperature dependence via the standard enthalpy of formation of  $Al_2O_3$  as obtained from the FactSage database. If  $\Delta_rG^0(T) < 0$ , the solid AlN phase is stable. The differently colored curves represent different levels of N2 background pressure. Following these results,

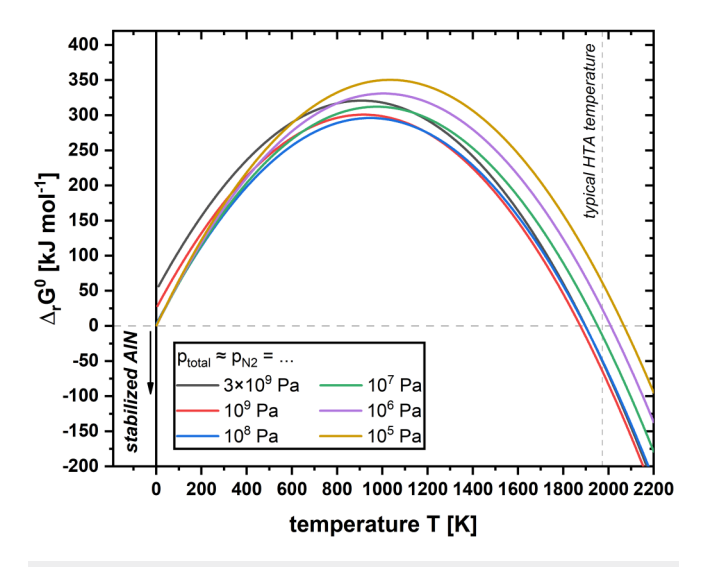


FIG. 5. Calculated reaction enthalpy of the chemical reaction shown in Eq. (1), using the equilibrium partial pressures obtained from the FactSage calculations. Stability of AIN is obtained at typically used HTA temperatures for nitrogen process pressures between 10<sup>6</sup> and 10<sup>7</sup> Pa.

a stable annealing process without the need for a proximity-cap or face-to-face approach may be expected for process pressures between 10<sup>6</sup> and 10<sup>7</sup> Pa. However, relatively fast heating rates are advisable to minimize the mass loss in the unstable regime during temperature ramp-up. The overall deviating behavior of  $\Delta_r G^0(T)$ for low temperature combined with  $p > 10^8$  Pa can be explained by the non-unity, continuously increasing activity of the solid AlN phase for these extremely high pressures as calculated from Eq. (6).

In summary, we applied the KEMS technique to measure partial pressures of aluminum and nitrogen species with a highquality AlN single crystal in the temperature regime relevant to HTA of AlN-on-sapphire templates. By fitting the temperaturedependent mass loss due to the congruent sublimation of AlN when annealed in an open-face configuration in a typical HTA furnace, it was possible to determine effective sublimation coefficients as used in the HLK equation. Based on the measured and confirmed equilibrium partial pressures, the Gibbs free energy of AlN formation as it is formulated in the FactSage database can be used to assess process conditions under which AlN decomposition is inhibited. Specifically, annealing under high N2 overpressures is expected to significantly suppress AlN decomposition and might allow for annealing in an open-face configuration.

#### V. CONCLUSIONS

Based on our experimental findings, the strong decomposition of AlN observed during high-temperature annealing under open-face conditions can be attributed to AlN approaching equilibrium between its gaseous and solid phases. Due to the comparably high equilibrium partial pressures of Al and N<sub>2</sub> above AlN and the low Al evaporates with a rate of ~5 nm/min, if annealed in an open-face 4 configuration at 1700 °C in N background pressure inside a typically used HTA furnace, solid AlN configuration at 1700 °C in  $N_2$ , at standard pressure. An increased  $\frac{3}{40}$  gas flux further accelerates the unwanted decomposition. If the partial pressure above AlN is compared to an established hightemperature ceramic, for example, Al<sub>2</sub>O<sub>3</sub> which may serve as the main furnace material, the difference in the equilibrium partial pressure by six orders of magnitude between Al above Al<sub>2</sub>O<sub>3</sub> and AlN is a huge obstacle for annealing AlN in an open-face configuration, if no measures are adopted to compensate the difference in partial pressure. Thus, following theoretical considerations, we propose an increase in the process pressure as a measure that allows the annealing of sapphire/AlN templates in an open-face configuration, without the detrimental etching of AlN. Cold-wall furnaces that support process pressures up to 10<sup>7</sup> Pa are commercially available and could be used to overcome the restricting face-to-face approach by compensating the low Al partial pressure with a high N2 overpressure. Ultimately, the presented results contribute to understanding the limitations of the HTA process and illustrate a path toward an industry-compatible batch process that mitigates the obstacles of a face-to-face configuration, enabling adoption in a high-volume production setting.

#### **ACKNOWLEDGMENTS**

This work was partly funded by Deutsche Forschungsgemeinschaft (DFG) in the framework of the SPP 2312 (Energieeffiziente Leistungselektronik "GaNius"), Project No. 462737320 (Aluminium

Nitrid für die vertikale Leistungselektronik) and also partly funded in the framework of Germany's Excellence Strategy—EXC-2123 QuantumFrontiers—No. 390837967.

#### **AUTHOR DECLARATIONS**

#### **Conflict of Interest**

The authors have no conflicts to disclose.

#### **Author Contributions**

Lukas Peters: Conceptualization (equal); Data curation (equal); Formal analysis (equal); Investigation (equal); Methodology (equal); Visualization (equal); Writing – original draft (equal); Writing – review & editing (equal). Dmitry Sergeev: Investigation (equal); Methodology (lead); Software (lead); Supervision (equal); Writing – review & editing (equal). Christoph Margenfeld: Methodology (equal); Writing – review & editing (equal). Michael Müller: Funding acquisition (equal); Project administration (equal); Supervision (equal); Writing – review & editing (equal). Andreas Waag: Funding acquisition (lead); Project administration (equal); Supervision (equal); Writing – review & editing (equal).

#### DATA AVAILABILITY

The data that support the findings of this study are available from the corresponding author upon reasonable request.

#### **REFERENCES**

- <sup>1</sup>M. Yamada, Y. Narukawa, and T. Mukai, Jpn. J. Appl. Physics: Lett., Part 2 **41**, L246-L248 (2002).
- <sup>2</sup>H. Amano, R. Collazo, C. De Santi, S. Einfeldt, M. Funato, J. Glaab, S. Hagedorn, A. Hirano, H. Hirayama, R. Ishii, Y. Kashima, Y. Kawakami, R. Kirste, M. Kneissl, R. Martin, F. Mehnke, M. Meneghini, A. Ougazzaden, P. J. Parbrook, S. Rajan, P. Reddy, F. Römer, J. Ruschel, B. Sarkar, F. Scholz, L. J. Schowalter, P. Shields, Z. Sitar, L. Sulmoni, T. Wang, T. Wernicke, M. Weyers, B. Witzigmann, Y. R. Wu, T. Wunderer, and Y. Zhang, J. Phys. D. Appl. Phys. 53, 503001 (2020).
- <sup>3</sup>M. Kneissl, T. Y. Seong, J. Han, and H. Amano, Nat. Photonics 13, 233 (2019). <sup>4</sup>M. Kneissl, in *III-Nitride Ultrav. Emit.*, edited by M. Kneissl, and J. Rass (Springer International Publishing, 2016), pp. 1–25.
- <sup>5</sup>K. Ban, J. I. Yamamoto, K. Takeda, K. Ide, M. Iwaya, T. Takeuchi, S. Kamiyama, I. Akasaki, and H. Amano, Appl. Phys. Express **4**, 052101 (2011).
- <sup>6</sup>J. Rass and N. Lobo-Ploch, in *III-Nitride Ultraviolet Emitters*, edited by M. Kneissl and J. Rass (Springer International Publishing, 2016), pp. 137–170.
- <sup>7</sup>L. Peters, C. Margenfeld, K. Jan, C. Ronning, and A. Waag, Phys. Status Solidi 2200485 (published online) (2022).
- <sup>8</sup>M. X. Wang, F. J. Xu, N. Xie, Y. H. Sun, B. Y. Liu, W. K. Ge, X. N. Kang, Z. X. Qin, X. L. Yang, X. Q. Wang, and B. Shen, Appl. Phys. Lett. **114**, 112105 (2019).
- <sup>9</sup>R. R. Sumathi, ECS J. Solid State Sci. Technol. **10**, 035001 (2021).
- <sup>10</sup>S. Hagedorn, S. Walde, A. Knauer, N. Susilo, D. Pacak, L. Cancellara, C. Netzel, A. Mogilatenko, C. Hartmann, T. Wernicke, M. Kneissl, and M. Weyers, Phys. Status Solidi Appl. Mater. Sci. 217, 1901022 (2020).
- <sup>11</sup>N. Tillner, C. Frankerl, F. Nippert, M. J. Davies, C. Brandl, R. Lösing, M. Mandl, H. J. Lugauer, R. Zeisel, A. Hoffmann, A. Waag, and M. P. Hoffmann, Phys. Status Solidi Basic Res. 257, 2000278 (2020).
- <sup>12</sup>H. Fukuyama, H. Miyake, G. Nishio, S. Suzuki, and K. Hiramatsu, Jpn. J. Appl. Phys. 55, 05FL02 (2016).
- <sup>13</sup>H. Miyake, C. H. Lin, K. Tokoro, and K. Hiramatsu, J. Cryst. Growth 456, 155 (2016).

- <sup>14</sup>N. Susilo, S. Hagedorn, D. Jaeger, H. Miyake, U. Zeimer, C. Reich, B. Neuschulz, L. Sulmoni, M. Guttmann, F. Mehnke, C. Kuhn, T. Wernicke, M. Weyers, and M. Kneissl, Appl. Phys. Lett. 112, 041110 (2018).
- <sup>15</sup>S. Liu, Y. Yuan, L. Huang, J. Zhang, T. Wang, T. Li, J. Kang, W. Luo, Z. Chen, X. Sun, and X. Wang, Adv. Funct. Mater. 32, 2112111 (2022).
- <sup>16</sup>D. L. Hildenbrand and W. F. Hall, J. Phys. Chem. **67**, 888 (1963).
- <sup>17</sup>D. Kobertz, C. Guguschev, and M. Müller, Open Thermodyn. J. 7, 71 (2013).
- <sup>18</sup>S. Hagedorn, S. Walde, A. Mogilatenko, M. Weyers, L. Cancellara, M. Albrecht, and D. Jaeger, J. Cryst. Growth 512, 142 (2019).
- 19C. W. Bale, E. Bélisle, P. Chartrand, S. A. Decterov, G. Eriksson, A. E. Gheribi, K. Hack, I. H. Jung, Y. B. Kang, J. Melançon, A. D. Pelton, S. Petersen, C. Robelin, J. Sangster, P. Spencer, and M. A. Van Ende, Calphad Comput. Coupling Phase Diagrams Thermochem. 54, 35 (2016).
- 20 C. Cheng, W. H. Lai, C. K. Huang, and C. Y. Liu, Ceram. Int. 46, 11080 (2020).
- <sup>21</sup>H. Miyake, G. Nishio, S. Suzuki, K. Hiramatsu, H. Fukuyama, J. Kaur, and N. Kuwano, Appl. Phys. Express **9**, 025501 (2016).
- <sup>22</sup>N. Jacobson, D. Kobertz, and D. Sergeev, Calphad Comput. Coupling Phase Diagrams Thermochem. 65, 111 (2019).
- 23 K. Hilpert, Rapid Commun. Mass Spectrom. 5, 175 (1991).
- <sup>24</sup>Z. H. Dong, D. Sergeev, D. Kobertz, N. D'Souza, S. Feng, M. Müller, and H. B. Dong, Metall. Mater. Trans. A Phys. Metall. Mater. Sci. 51, 309 (2020).
- 25D. Kobertz, M. Müller, and A. Molak, Calphad Comput. Coupling Phase Diagrams Thermochem. 46, 62 (2014).
- <sup>26</sup>D. Sergeev, E. Yazhenskikh, D. Kobertz, and M. Müller, Calphad Comput. Coupling Phase Diagrams Thermochem. 65, 42 (2019).
- <sup>27</sup>K. L. Bell, H. B. Gilbody, J. G. Hughes, A. E. Kingston, and F. J. Smith, J. Phys. Chem. Ref. Data 12, 891 (1983).
- <sup>28</sup>J. Drowart, C. Chatillon, J. Hastie, and D. Bonnell, Pure Appl. Chem. 77, 683 (2005).
- <sup>29</sup>A. H. Persad and C. A. Ward, Chem. Rev. 116, 7727 (2016).
- 30 C. Hartmann, L. Matiwe, J. Wollweber, I. Gamov, K. Irmscher, M. Bickermann, and T. Straubinger, CrystEngComm 22, 1762 (2020).
- <sup>31</sup>C. Hartmann, J. Wollweber, S. Sintonen, A. Dittmar, L. Kirste, S. Kollowa, K. Irmscher, and M. Bickermann, CrystEngComm 18, 3488 (2016).
- 32G. Meloni and K. A. Gingerich, J. Chem. Phys. 113, 10978 (2000).
- <sup>33</sup>L. Andrews, M. Zhou, G. V. Chertihin, W. D. Bare, and Y. Hannachi, J. Phys. Chem. A **104**, 1656 (2000).
- <sup>34</sup>M. Berglund and M. E. Wieser, Pure Appl. Chem. **83**, 397 (2010).
- 35L. H. Dreger, V. V. Dadape, and J. L. Margrave, J. Phys. Chem. 66, 1556 (1962)
- <sup>36</sup>A. S. Segal, S. Y. Karpov, Y. N. Makarov, E. N. Mokhov, A. D. Roenkov, M. G. Ramm, and Y. A. Vodakov, J. Cryst. Growth 211, 68 (2000).
- <sup>37</sup>T. Prohaska, J. Irrgeher, J. Benefield, J. K. Böhlke, L. A. Chesson, T. B. Coplen, T. Ding, P. J. H. Dunn, M. Gröning, N. E. Holden, H. A. J. Meijer, H. Moossen, A. Possolo, Y. Takahashi, J. Vogl, T. Walczyk, J. Wang, M. E. Wieser, S. Yoneda, X. K. Zhu, and J. Meija, Pure Appl. Chem. 94, 573 (2022).
- <sup>38</sup>M. Hoch and D. Ramakrishnan, J. Electrochem. Soc. **118**, 1204 (1971).
- <sup>39</sup>P. M. Dryburgh, J. Cryst. Growth **125**, 65 (1992).
- <sup>40</sup>S. Hagedorn, A. Mogilatenko, S. Walde, D. Pacak, J. Weinrich, C. Hartmann, and M. Weyers, Phys. Status Solidi 258, 2100187 (2021).
- <sup>41</sup>D. Wang, K. Uesugi, S. Xiao, K. Norimatsu, and H. Miyake, Appl. Phys. Express 14, 035505 (2021).
- 42<sup>M</sup>. Nishitsuji and F. Hasegawa, Jpn. J. Appl. Phys. 28, L895 (1989).
- 43 H. Fujino, E. Kume, and S. Sakai, Phys. C 426-431, 1474 (2005).
- 44U. König, J. Hilgarth, and H.-H. Tiemann, J. Electron. Mater. 14, 311 (1985).
- 45 J. A. Del Alamo and T. Mizutani, J. Appl. Phys. 62, 3456 (1987).
- <sup>46</sup>A. Babiński, J. Jasiński, R. Bożek, A. Szepielow, and J. M. Baranowski, Appl. Phys. Lett. **79**, 2576 (2001).
- <sup>47</sup>K. Sierakowski, R. Jakiela, B. Lucznik, P. Kwiatkowski, M. Iwinska, M. Turek, H. Sakurai, T. Kachi, and M. Bockowski, Electronics 9, 1380 (2020).